Letter

Spin nematics meet spin liquids: Exotic quantum phases in the spin-1 bilinear-biquadratic model with Kitaev interactions

Rico Pohle,[1] Nic Shannon,[2] and Yukitoshi Motome[1]

[1]*Department of Applied Physics, University of Tokyo, Hongo, Bunkyo-ku, Tokyo 113-8656, Japan*

[2]*Theory of Quantum Matter Unit, Okinawa Institute of Science and Technology Graduate University, Onna-son, Okinawa 904-0412, Japan*

(Received 19 December 2022; revised 6 March 2023; accepted 20 March 2023; published 4 April 2023)

Spin liquid crystals are magnetic analogs of liquid crystals, possessing properties of both liquids and solids, a typical example of which are spin nematics. Spin nematics share many features with spin liquids, and the interplay between them is a promising, but little explored, route to uncovering new phases of matter. Here, we address this question in the context of a spin-1 magnet on the honeycomb lattice, by considering a model with both biquadratic interactions, favoring spin-nematic states, and Kitaev-like interactions, supporting spin liquids. Accompanying these, where dipole and quadrupole moments compete, we find a plethora of exotic phases, including multiple-q states with nonzero scalar spin chirality, a quasi-one-dimensional coplanar phase, a twisted conical phase, and a noncoplanar order state which gives way to a chiral spin liquid at finite temperature. The implication of these results for experiment is discussed.

DOI: 10.1103/PhysRevB.107.L140403

Introduction. Liquid crystals form a state of matter which contains properties of both liquids and solids [1–3]. Well-known for their fascinating "Schlieren" textures, the nematic phase of an organic liquid crystal is made of rod-shaped molecules which align themselves along a particular axis, while still flowing like a liquid with the absence of crystalline positional order [4,5]. Their magnetic analogs, called spin liquid crystals, are spin states in magnets which show similar phenomena. A typical example is the spin nematic state where localized magnetic quadrupole moments act like rod-shaped molecules and form orientational order without any long-range magnetic dipole order [6,7–11]. Such nematic states have attracted much attention as "hidden magnetic orders" since they are hard to detect with conventional scattering experiments [12–15].

Spin liquids represent another family of spin states which are hard to detect due to the absence of conventional long-range magnetic order [16–20]. Strong competition between magnetic interactions frustrates the system to form a liquid-like state made of spins on the lattice. Such states are of particular interest, since they are accompanied by emergent gauge fields, topological order, and fractionalized excitations, defying a conventional description within the Landau paradigm of magnetism [21–24].

The central question we address in this study is "What happens when a spin nematic and a spin liquid meet?" While both states stay "hidden" for conventional magnetic probes, their fundamental properties manifest in different ways: The spin nematic breaks spin rotation symmetry and shows collective magnetic excitations associated with quadrupolar order, whereas the spin liquid shows no conventional symmetry breaking, with magnetic excitations forming a continuum associated with fractional quasiparticles. The interplay between spin-nematic and spin-liquid phases offers a promising route to uncovering other unconventional phases, and phase transitions in both classical [25–27] and quantum spin models [28–32]. However, to date, this interesting problem remains largely unexplored because of the technical difficulty of solving models which support such "hidden" phases.

In this Letter, we explore what happens when spin liquids meet spin nematics in a spin-1 magnet on the honeycomb lattice. We consider a bilinear-biquadratic (BBQ) model, extended through anisotropic Kitaev-type interactons. The biquadratic interactions stabilize spin nematic phases with dominant quadrupole character [33]. Meanwhile, the Kitaev interactions stabilize the so-called Kitaev spin liquid [34], which has been extensively studied for an effective spin-orbital entangled moment $S = 1/2$ [35–39], and its recent extension to higher S in theory and experiment [40–47]. We reveal that the competition between the positive biquadratic interaction and the Kitaev interaction promotes unconventional phases by mixing dipoles and quadrupoles to alleviate strong frustration.

Ground-state phase diagram. We solve the BBQ model under influence of Kitaev interactions for $S = 1$ magnetic moments on the honeycomb lattice:

$$\mathcal{H}_{\mathsf{BBQ-K}} = \sum_{\langle i,j\rangle}[J_1\, \mathbf{S}_i \cdot \mathbf{S}_j + J_2\, (\mathbf{S}_i \cdot \mathbf{S}_j)^2] + K \sum_{\alpha=x,y,z} \sum_{\langle ij\rangle_\alpha} S_i^\alpha S_j^\alpha\,, \tag{1}$$

where J_1, J_2, and K respectively account for the Heisenberg (bilinear), biquadratic, and Kitaev interaction strengths on nearest-neighbor bonds. The index α selects the spin- and bond-anisotropic Kitaev interactions on the honeycomb lattice [34]. We parametrize the model by normalizing the total interaction strength as

$$(J_1, J_2, K) = (\sin\theta\cos\phi, \sin\theta\sin\phi, \cos\theta). \tag{2}$$

 ©2023 American Physical Society

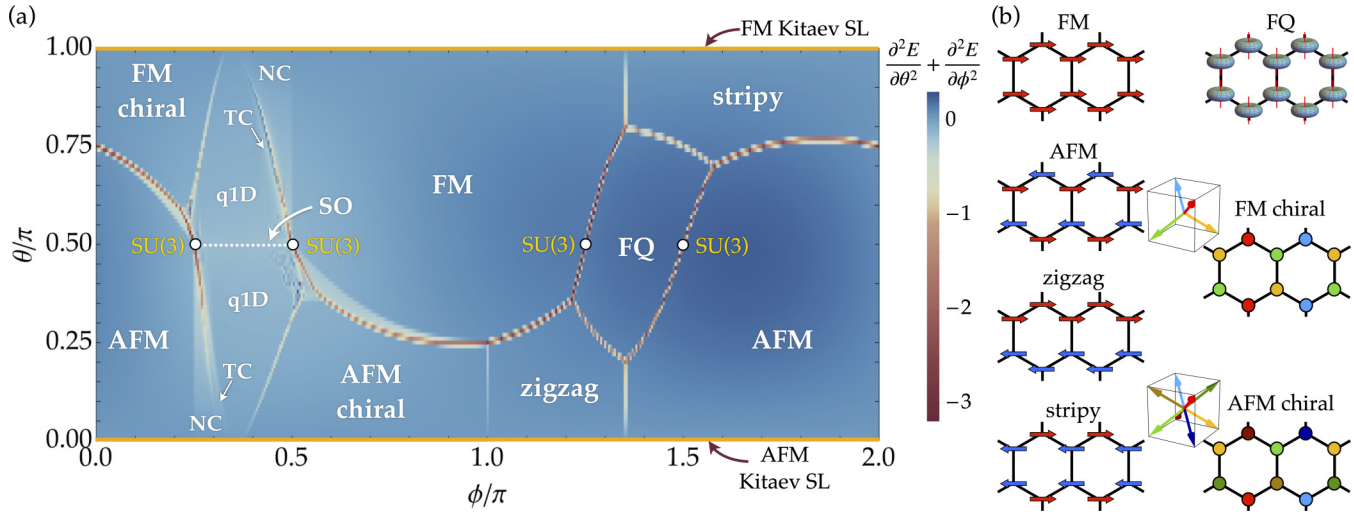

FIG. 1. Ground states of $\mathcal{H}_{\mathsf{BBQ-K}}$ in Eq. (1), obtained by variational energy minimization for a finite-size cluster with $N = 28\,800$ spins under periodic boundary conditions. (a) 2D equirectangular projection of the full phase diagram as a function of θ and ϕ. We plot the second derivative of the internal energy by the contour color to make the phase boundaries visible. (b) Real-space configurations of the dominant ordered phases in (a). For negative J_2 ($1.0 < \phi/\pi < 2.0$) the model stabilizes magnetic dipolar orders, such as ferromagnetic (FM), antiferromagnetic (AFM), zigzag, and stripy orders, in addition to spin-nematic ferroquadrupolar (FQ) order. Meanwhile, for positive J_2 ($0.0 < \phi/\pi < 1.0$) the competition between chiral magnetic order, the Kitaev spin liquid (SL), and quadrupolar semiorder (SO) gives rise to unconventional phases, such as the twisted conical (TC), quasi-one-dimensional (q1D) coplanar, and noncoplanar (NC) ordered phases. Details of those unconventional phases will be shown in Fig. 2.

In this form, $\mathcal{H}_{\mathsf{BBQ-K}}$ recovers the well-known limits of the BBQ model on the equator, $\theta/\pi = 0.5$ ($K = 0$); the AFM Kitaev model at the north pole, $\theta/\pi = 0$ ($K = 1$, $J_1 = J_2 = 0$); the FM Kitaev model at the south pole, $\theta/\pi = 1$ ($K = -1$, $J_1 = J_2 = 0$); and the Kitaev-Heisenberg model at $\phi/\pi = 0$ or 1 ($J_2 = 0$).

To study the ground-state and finite-temperature properties of $\mathcal{H}_{\mathsf{BBQ-K}}$ in Eq. (1), we utilize a recently developed U(3) formalism [48]. By embedding the underlying $\mathfrak{su}(3)$ algebra of $S = 1$ moments into the larger $\mathfrak{u}(3)$ algebra with an additional spin-length constraint, we are able to treat quantum aspects of the problem exactly at the level of a single site, namely, simultaneously access dipole and quadrupole fluctuations, despite the drawback of loosing quantum entanglement across the lattice (see technical details in the Supplemental Material [49]). This approach is equivalent to the formalism of SU(3) coherent states [50], which can be generalized to any arbitrary Lie Group SU(N) [51–54].

In Fig. 1(a) we show the ground-state phase diagram of $\mathcal{H}_{\mathsf{BBQ-K}}$, obtained from large-scale variational energy minimization, using the machine learning library JAX [55,56] for a sufficiently large cluster with $N_s = 2L^2 = 28800$ spins ($L = 120$) under periodic boundary conditions. To visualize phase boundaries, we plot $\partial^2 E/\partial\theta^2 + \partial^2 E/\partial\phi^2$, the sum of the second derivatives of the internal energy E with respect to θ and ϕ.

Where the biquadratic interaction J_2 is negative ($1.0 < \phi/\pi < 2.0$), we recover a combination of phases previously reported in the $S = 1$ Kitaev-Heisenberg model [41,43] and the BBQ model [33]. These comprise dipolar order, in the form of ferromagnetic (FM), antiferromagnetic (AFM), zigzag, and stripy phases [41,43], together with a ferroquadrupolar (FQ) spin nematic, stabilized by the biquadratic interaction [33]. Corresponding real-space spin configurations are shown in Fig. 1(b), with dipole moments depicted as arrows, and quadrupole moments as "doughnut-shaped" spin-probability distributions [9,10].

In contrast, where the biquadratic interaction J_2 is positive ($0.0 < \phi/\pi < 1.0$), we find a number of unconventional phases which emerge from the competition between frustrated interactions. Adjacent to the zigzag and stripy phases, we find FM and AFM chiral phases, which are noncoplanar dipolar-ordered phases with net scalar spin chirality, $|\kappa| = 8/(3\sqrt{3})$ and $|\kappa| = 16/(3\sqrt{3})$ in the regions for $\theta/\pi > 0.5$ and $\theta/\pi < 0.5$, respectively (see definition of κ in the Supplemental Material [49]). These chiral phases are triple-q states with eight-sublattice order, also known as "tetrahedral" and "cubic" states [57], in which spins point to the corners of a unit cube [see Fig. 1(b)] [58]. We note that the stripy and FM chiral (zigzag and AFM chiral) states are energetically degenerate along the vertical line at $\phi/\pi = 0$ ($\phi/\pi = 1$) for $\theta/\pi \geqslant 0.75$ ($\theta/\pi \leqslant 0.25$). This degeneracy is lifted by thermal fluctuations, which select the stripy (zigzag) phase, consistent with DMRG results for the spin–1 Kitaev–Heisenberg model [43].

Competing region between dipoles and quadrupoles. Between FM, AFM, and chiral ordered phases, dipole and quadrupole moments mix in nontrivial ways and we find a range of exotic phases. These results are summarized in Fig. 2(a), where the color bar shows the expectation value of the magnitude of the dipole moment $|\mathbf{S}| = \sum_i |\mathbf{S}_i|/N_s$. In the limit of the BBQ model ($\theta/\pi = 0.5$), a purely quadrupolar state with $|\mathbf{S}| = 0$ is realized, connecting the two SU(3) points at $\phi/\pi = 0.25$ and $\phi/\pi = 0.5$. This state is known to be semiordered (SO) (or semidisordered) [8,59], with $\langle \mathbf{S}_i \cdot \mathbf{S}_j \rangle = 0$ for all the bonds to minimize $\mathcal{H}_{\mathsf{BBQ}}$ with positive J_1 and J_2. We note that this state was claimed to be replaced by a plaquette valence bond crystal when quantum entanglement is fully taken into account [60]. Introducing the Kitaev

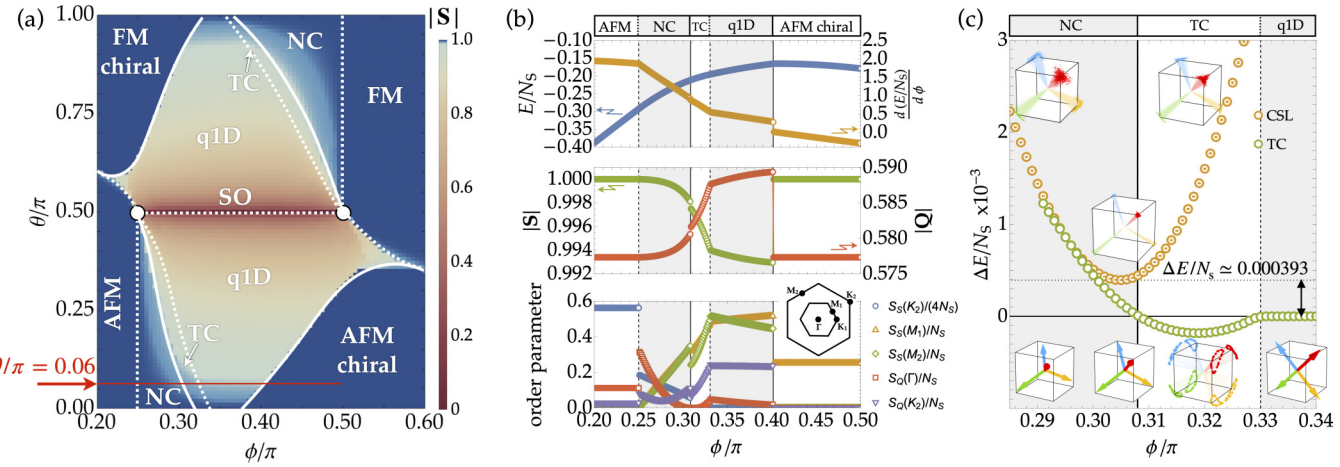

FIG. 2. Competing region between dipoles and quadrupoles. (a) Averaged spin norm $|\mathbf{S}|$ plotted in the range of $0.2 < \phi/\pi < 0.6$. The solid and dashed lines represent first- and second-order phase boundaries, respectively. (b) Normalized energy and its derivative, E/N_s and $\partial(E/N_s)/\partial\phi$, respectively, which visualize the boundaries between the antiferromagnet (AFM), noncoplanar order (NC), twisted conical (TC), quasi-one-dimensional (q1D), coplanar, and AFM chiral states (top); spin and quadrupole norms, $|\mathbf{S}|$ and $|\mathbf{Q}|$, respectively (middle), and the structure factors for dipole and quadrupole moments, $S_S(\mathbf{q})$ and $S_Q(\mathbf{q})$, respectively, at high-symmetry momenta (bottom) at $\theta/\pi = 0.06$ [red line in (a)]. (c) Energy measured from the NC state at $\theta/\pi = 0.06$. The lower insets show spin configurations in each ordered phase, while the upper ones represent metastable states of a chiral spin liquid (CSL).

interaction $|K|$ ($\theta/\pi \neq 0.5$) immediately induces the formation of a nonzero dipole moment $|\mathbf{S}| \neq 0$. Under the orthogonal conditions of $\langle \mathbf{S}_i \cdot \mathbf{S}_j \rangle = 0$, the Kitaev interaction prefers a coplanar state with dipoles aligned within the xy, yz, or zx plane, in which the Kitaev energy is minimized on two bonds while leaving the third one to be zero. Hence, dominant correlations prevail along isolated chains and stabilize a coplanar, quasi-one-dimensional (q1D) state in an extended region away from the BBQ limit [see Fig. 2(a)]. The appearance of small quadrupolar correlations will induce a weak interchain coupling to form two-dimensional order.

Sandwiched between the q1D coplanar phase and the AFM/FM ordered phase, $\mathcal{H}_{\mathsf{BBQ-K}}$ minimizes its energy by forming spin textures with noncoplanar (NC) orientation. In Fig. 2(b) we show physical observables along a cut with $\theta/\pi = 0.06$ [red line in Fig. 2(a)], visiting AFM, NC, twisted conical (TC), q1D coplanar, and AFM chiral phases. Phase boundaries are easily distinguished from the first derivative of energy $d(E/N_s)/d\phi$ [top panel of Fig. 2(b)]. Each phase has been identified from the spin and quadrupole norms, $|\mathbf{S}|$ and $|\mathbf{Q}|$ shown in the middle panel of Fig. 2(b), and their order parameters, measured from the structure factors $S_S(\mathbf{q})$ for dipoles and $S_Q(\mathbf{q})$ for quadrupoles at high symmetry momenta, Γ, K_1, K_2, M_1, and M_2, shown in the bottom panel of Fig. 2(b) (see definitions in the Supplemental Material [49]).

By increasing $\phi/\pi > 0.25$, spins start to cant away from the collinear AFM arrangement until they point almost along the corners of a unit cube for $\phi/\pi \approx 0.305$, as shown in the lower inset of Fig. 2(c). For $\phi/\pi \gtrsim 0.308$, the ground state becomes a four-sublattice conical state, where spins process around two corners of a unit cube. This precession, however, is not circular, but rather shows a twist with a node between those two corners, which led us to call this state TC. Further increase of ϕ makes the cones shrink and smoothly merge with the q1D coplanar state at $\phi/\pi \gtrsim 0.330$. Near the transition between the NC and TC phases, we observe a metastable noncoplanar state in the energy minimization, whose energy minimum is just $\Delta E/N_s \simeq 0.000393$ above the NC ground state. Interestingly, we obtain many different noncoplanar spin states with almost the same energy, which, in fact, form an extensively degenerate chiral spin liquid (CSL).

Eight-color chiral spin liquid. The extensive degeneracy of the CSL is transparently understood by two simplifications. One is to assume $|\mathbf{S}| = 1$, the other is to allow for only eight discrete spin states which exactly point to the corners of a unit cube. Such simplifications are justified since the metastable states are dominantly made of dipoles and their spins gather around the corners, as seen in the upper insets of Fig. 2(c). Under these simplifications, positive J_1 and J_2 select only four out of eight discrete spin states, which we identify by color, as indicated in the inset of Fig. 3(a) (or equivalently the other four spins with opposite directions). Then, the Kitaev interactions enforce bond constraints, which

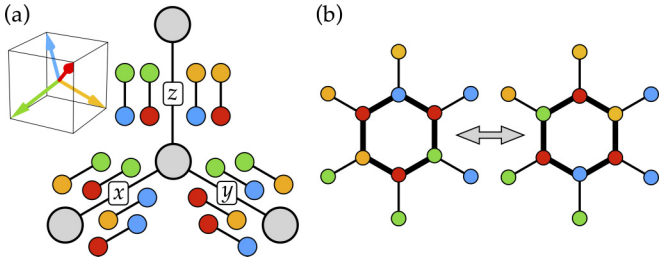

FIG. 3. Macroscopic degeneracy in the eight-color chiral spin liquid (CSL). (a) Spin and bond constraints allow for only four color pairs on individual Kitaev bonds. Inset assigns colors to spins perfectly pointing to the corners of the unit cube. (b) While respecting the constraints in (a), the CSL manifold allows for pairs of spin states per hexagon, which are related by a six-spin cluster update. All allowed hexagon configurations are shown in the Supplemental Material [49].

allow for only four combinations of color pairs per bond, where their explicit combination differs between the three Kitaev bonds, as illustrated in Fig. 3(a). These local bond constraints are not strong enough to enforce long-range order, instead form a manifold with macroscopic degeneracy, always allowing for two spin configurations per hexagon [see Fig. 3(b)]. The number of states respecting the constraints in Fig. 3(a) per hexagon is 64 (see the Supplemental Material [49]), leading to a residual entropy of $S/N_s = \frac{1}{2}\log 2$, which is 1/6 of the total entropy of the system, $S/N_s = \log 8$. We find that the degenerate manifold gives rise to a nonzero scalar spin chirality; $|\kappa| = 1/\sqrt{3}$, hence justifying its name as the eight-color CSL. Since the CSL is a metastable state [see Fig. 2(c)], we expect an entropy-driven phase transition from the NC state to the eight-color CSL by raising the temperature. This motivates us to perform finite-temperature Monte Carlo simulations of $\mathcal{H}_{\mathrm{BBQ-K}}$ within the U(3) formalism, henceforth called "u3MC" [48] (see technical details in the Supplemental Material [49]).

In Fig. 4 we show u3MC results at $\theta/\pi = 0.06$ and $\phi/\pi = 0.305$, where the energy difference ΔE to the NC ground state shows a minimum [see Fig. 2(c)]. The specific heat in Fig. 4(a) shows two singularities at $T_1 = 0.0055(2)$ and $T_2 = 0.0017(2)$. Below T_1 we obtain a nonzero scalar spin chirality, while we do not see any Bragg peaks in the structure factors for both dipole and quadrupole sectors; see the dipole one in the middle panel of Fig. 4(d) and the quadrupole one in the Supplemental Material [49]. Hence, we associate T_1 with a discrete Z_2 chiral symmetry breaking from the high-temperature cooperative paramagnetic state, which retains a classical AFM Kitaev spin liquid feature as shown in the right panel of Fig. 4(d) [61] (see the Supplemental Matarial [49]), into the CSL. The bond constraints, explained in Fig. 3, lead us to compute the $S = 1$ semiclassical analog of the Z_2-flux operator [34]: $W_p = \prod_{j\in p}\sqrt{3}S_j^{\mu}$ on hexagons p. As plotted in Fig. 4(c), W_p rapidly increases below $T \sim 0.01$ and becomes nearly one in the CSL below T_1, suggesting that the CSL accompanies "flux order" like in the Kitaev SL. With further decrease of temperature, below T_2, we find characteristic Bragg peaks corresponding to NC order as shown in the left panel of Fig. 4(d), and hence associate T_2 with a symmetry breaking into the NC ordered phase. Although the estimate of T_2 is not fully reliable because of the slowing down of u3MC simulations in the low temperature regime, it compares well with the free energy $\frac{\Delta E}{S} \approx 0.001 \approx T_2$, given $\Delta E/N_s \simeq 0.000393$ and the entropy of the CSL manifold $S/N_s = \frac{1}{2}\log 2 \simeq 0.347$. Thus, we identify the CSL to be driven by the entropy associated with the macroscopic degeneracy discussed in Fig. 3. We further confirmed that the intermediate-temperature CSL prevails in an extended region around $\phi/\pi \sim 0.3$ and $0 < \theta/\pi \lesssim 0.2$ (see the Supplemental Material [49]).

Conclusions and discussions. To answer the question "What happens when a spin nematic and a spin liquid meet?", we have theoretically investigated the spin $S = 1$ bilinear-biquadratic model on the honeycomb lattice with Kitaev-type anisotropic interactions. In the pure Kitaev limit we recovered the semiclassical analog of the $S = 1$ Kitaev spin liquid, which was suggested to emerge in honeycomb materials with Ni^{2+} ions [41]. The limit of strong nega-

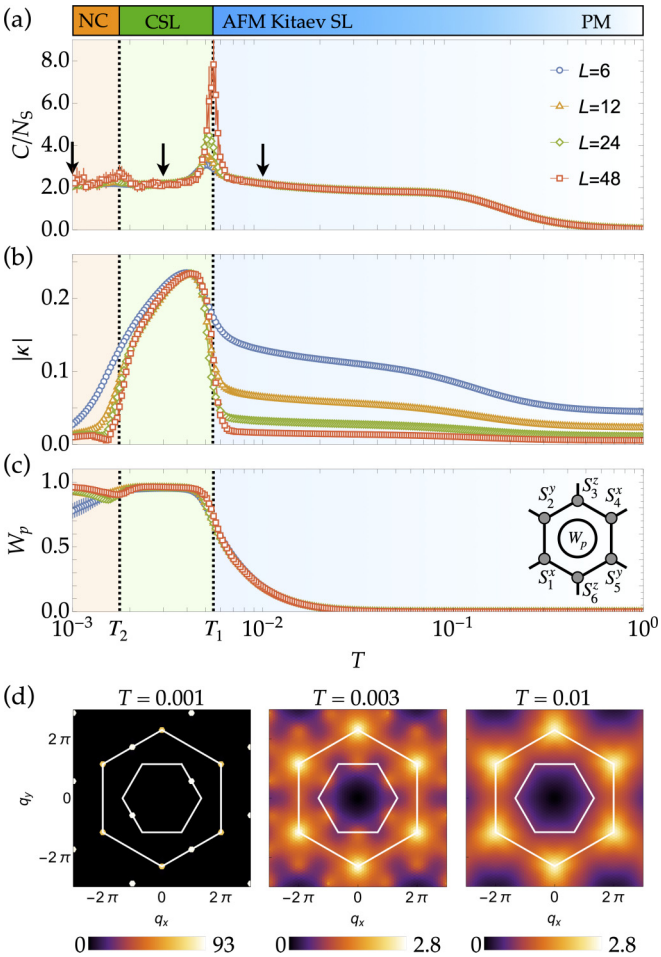

FIG. 4. Finite-temperature Monte Carlo results at $\theta/\pi = 0.06$ and $\phi/\pi = 0.305$ where the ground state is NC ordered. Shown are T dependences of (a) the specific heat per site, (b) the absolute value of the scalar spin chirality per site, $|\kappa|$, and (c) the $S = 1$ semiclassical analog of the Z_2-flux operator. The data are taken for $L = 6$, 12, 24, and 48 ($N_s = 72$, 288, 1152, and 4608). (d) Spin structure factor $S_S(\mathbf{q})$ at temperatures indicated with black arrows in (a), for $L = 12$ at $T = 0.001$ and $L = 24$ at $T = 0.003$ and 0.01.

tive biquadratic interactions revealed a ferroquadrupolar spin nematic state, which can be expected in materials with spin-phonon coupling [62–64]. By tuning model parameters to positive biquadratic interactions, which are expected in materials with orbital degeneracy [65–67], we observed the formation of triple-q ordered phases with net scalar spin chirality. Note that a similar state was found for the Kitaev-Heisenberg model in a magnetic field [68] and the honeycomb material $Na_2Co_2TeO_6$ [69–71]. Deep in the frustrated region, spin dipole and quadrupole components mix and promote quasi-one-dimensional coplanar ordered phases, unconventional noncoplanar and conical phases, and a finite-temperature eight-color chiral spin liquid phase retaining the Kitaev spin liquid feature of flux order. Such exotic phases survive for large Kitaev anisotropy offering an opportunity for them to emerge as perturbation in higher-S Kitaev magnets [41,44,46].

The results in this Letter were derived within a semiclassical approximation which does not take into account entanglement between spins. A drawback of this approach is that Kitaev-like spin-liquid behavior is found only exactly at the north and south poles, while in a fully quantum treatment, it is expected to be an extended phase [72]. Nonetheless, comparison with DMRG results for the spin-1 Kitaev-Heisenberg model [43] reveals an encouraging level of agreement, with the same phases identified, and only small changes in the numerical values of phase boundaries.

While the $S = 1/2$ Kitaev model offers a bond-nematic state near the Kitaev spin liquid [73], the physics in $S = 1$ Kitaev magnets appears to be much richer. The enlarged local Hilbert space allows for on-site multipole fluctuations, which work as an additional degree of freedom to minimize local bond energies by forming unconventional quantum states of matter. Similar exotic examples have recently been shown to exist in CP^2 skyrmion crystals [74,75], on triangular magnets [76,77], and in spin-orbital Mott insulators [78]. The possibilities to find novel phases in multipolar magnets are vast and the recent development of suitable numerical methods [48,52–54] allows us to access and study them in a controlled way. We hope our findings will stimulate further theoretical and experimental exploration of multipolar magnets and their exotic quantum phases formed from the interplay between spin nematics and spin liquids.

Acknowledgments. The authors are pleased to acknowledge helpful conversations with Yutaka Akagi, Yuki Amari, Koji Inui, Lukas Janssen, Yasuyuki Kato, and Kotaro Shimizu. This work was supported by Japan Society for the Promotion of Science (JSPS) KAKENHI Grants No. JP19H05822 and No. JP19H05825, and the Theory of Quantum Matter Unit, OIST. Numerical calculations we carried out using HPC facilities provided by the Supercomputer Center of the Institute for Solid State Physics, the University of Tokyo.

[1] H. Kelker, Mol. Cryst. Liq. Cryst. **21**, 1 (1973).
[2] H. Kelker, Mol. Cryst. Liq. Cryst. Inc. Nonlinear Opt. **165**, 1 (1988).
[3] P. de Gennes and J. Prost, *The Physics of Liquid Crystals*, International Series of Monographs on Physics (Clarendon Press, Oxford, 1993).
[4] N. D. Mermin and H. Wagner, Phys. Rev. Lett. **17**, 1133 (1966).
[5] G. P. Alexander, B. G.-g. Chen, E. A. Matsumoto, and R. D. Kamien, Rev. Mod. Phys. **84**, 497 (2012).
[6] M. Blume and Y. Y. Hsieh, J. Appl. Phys. **40**, 1249 (1969).
[7] V. M. Matveev, JETP **38**, 813 (1974).
[8] N. Papanicolaou, Nucl. Phys. B **305**, 367 (1988).
[9] H. Tsunetsugu and M. Arikawa, J. Phys. Soc. Jpn. **75**, 083701 (2006).
[10] A. Läuchli, F. Mila, and K. Penc, Phys. Rev. Lett. **97**, 087205 (2006).
[11] K. Penc and A. M. Läuchli, Spin nematic phases in quantum spin systems, in *Introduction to Frustrated Magnetism: Materials, Experiments, Theory*, edited by C. Lacroix, P. Mendels, and F. Mila (Springer, Berlin, Heidelberg, 2011), pp. 331–362.
[12] A. F. Andreev and I. A. Grishchuk, JETP **60**, 267 (1984).
[13] A. Smerald, H. T. Ueda, and N. Shannon, Phys. Rev. B **91**, 174402 (2015).
[14] A. Smerald and N. Shannon, Phys. Rev. B **93**, 184419 (2016).
[15] Y. Kohama, H. Ishikawa, A. Matsuo, K. Kindo, N. Shannon, and Z. Hiroi, Proc. Natl. Acad. Sci. **116**, 10686 (2019).
[16] C. Lacroix, P. Mendels, and F. Mila, *Introduction to Frustrated Magnetism: Materials, Experiments, Theory* (Springer, Berlin, Heidelberg, 2011).
[17] H. T. Diep, *Frustrated Spin Systems*, 2nd ed. (World Scientific, Singapore, 2013).
[18] M. Udagawa and L. Jaubert, *Spin Ice* (Springer International Publishing, Cham, 2021).
[19] J. Wen, S.-L. Yu, S. Li, W. Yu, and J.-X. Li, npj Quantum Mater. **4**, 12 (2019).
[20] C. Broholm, R. J. Cava, S. A. Kivelson, D. G. Nocera, M. R. Norman, and T. Senthil, Science **367**, eaay0668 (2020).
[21] X.-G. Wen, Phys. Rev. B **65**, 165113 (2002).
[22] L. Balents, Nature (London) **464**, 199 (2010).
[23] L. Savary and L. Balents, Rep. Prog. Phys. **80**, 016502 (2016).
[24] Y. Zhou, K. Kanoda, and T.-K. Ng, Rev. Mod. Phys. **89**, 025003 (2017).
[25] J. T. Chalker, P. C. W. Holdsworth, and E. F. Shender, Phys. Rev. Lett. **68**, 855 (1992).
[26] N. Shannon, K. Penc, and Y. Motome, Phys. Rev. B **81**, 184409 (2010).
[27] M. Taillefumier, O. Benton, H. Yan, L. D. C. Jaubert, and N. Shannon, Phys. Rev. X **7**, 041057 (2017).
[28] R. Shindou and T. Momoi, Phys. Rev. B **80**, 064410 (2009).
[29] T. Grover and T. Senthil, Phys. Rev. Lett. **107**, 077203 (2011).
[30] O. Benton, L. D. C. Jaubert, R. R. P. Singh, J. Oitmaa, and N. Shannon, Phys. Rev. Lett. **121**, 067201 (2018).
[31] W.-J. Hu, S.-S. Gong, H.-H. Lai, H. Hu, Q. Si, and A. H. Nevidomskyy, Phys. Rev. B **100**, 165142 (2019).
[32] H.-J. Yang, N. Shannon, and S. B. Lee, Phys. Rev. B **104**, L100403 (2021).
[33] H. H. Zhao, C. Xu, Q. N. Chen, Z. C. Wei, M. P. Qin, G. M. Zhang, and T. Xiang, Phys. Rev. B **85**, 134416 (2012).
[34] A. Kitaev, Ann. Phys. **321**, 2 (2006).
[35] G. Jackeli and G. Khaliullin, Phys. Rev. Lett. **102**, 017205 (2009).
[36] L. Janssen and M. Vojta, J. Phys.: Condens. Matter **31**, 423002 (2019).
[37] H. Takagi, T. Takayama, G. Jackeli, G. Khaliullin, and S. E. Nagler, Nat. Rev. Phys. **1**, 264 (2019).
[38] Y. Motome and J. Nasu, J. Phys. Soc. Jpn. **89**, 012002 (2020).
[39] S. Trebst and C. Hickey, Phys. Rep. **950**, 1 (2022).
[40] G. Baskaran, D. Sen, and R. Shankar, Phys. Rev. B **78**, 115116 (2008).
[41] P. P. Stavropoulos, D. Pereira, and H.-Y. Kee, Phys. Rev. Lett. **123**, 037203 (2019).
[42] A. Scheie, K. Ross, P. P. Stavropoulos, E. Seibel, J. A. Rodriguez-Rivera, J. A. Tang, Y. Li, H.-Y. Kee, R. J. Cava, and C. Broholm, Phys. Rev. B **100**, 214421 (2019).
[43] X.-Y. Dong and D. N. Sheng, Phys. Rev. B **102**, 121102(R) (2020).

[44] K. Fukui, Y. Kato, J. Nasu, and Y. Motome, Phys. Rev. B **106**, 174416 (2022).

[45] H.-K. Jin, W. M. H. Natori, F. Pollmann, and J. Knolle, Nat. Commun. **13**, 3813 (2022).

[46] A. Rayyan, D. Churchill, and H.-Y. Kee, Phys. Rev. B **107**, L020408 (2023).

[47] K. M. Taddei, V. O. Garlea, A. M. Samarakoon, L. D. Sanjeewa, J. Xing, T. W. Heitmann, C. D. Cruz, A. S. Sefat, and D. Parker, Phys. Rev. Res. **5**, 013022 (2023).

[48] K. Remund, R. Pohle, Y. Akagi, J. Romhányi, and N. Shannon, Phys. Rev. Res. **4**, 033106 (2022).

[49] See Supplemental Material at http://link.aps.org/supplemental/10.1103/PhysRevB.107.L140403 for details of the method, eight-color chiral spin liquid, the semiclassical analog of the $S = 1$ Kitaev spin liquid, and details of triple-q ordered phases, which includes Refs. [9,10,48,50–56,61,79–83].

[50] S. Gnutzmann and M. Kus, J. Phys. A: Math. Gen. **31**, 9871 (1998).

[51] A. M. Perelomov, Commun. Math. Phys. **26**, 222 (1972).

[52] H. Zhang and C. D. Batista, Phys. Rev. B **104**, 104409 (2021).

[53] D. Dahlbom, H. Zhang, C. Miles, X. Bai, C. D. Batista, and K. Barros, Phys. Rev. B **106**, 054423 (2022).

[54] D. Dahlbom, C. Miles, H. Zhang, C. D. Batista, and K. Barros, Phys. Rev. B **106**, 235154 (2022).

[55] J. Bradbury, R. Frostig, P. Hawkins, M. J. Johnson, C. Leary, D. Maclaurin, G. Necula, A. Paszke, J. VanderPlas, S. Wanderman-Milne, and Q. Zhang, JAX: Composable transformations of Python+NumPy programs, version 0.3.13 (2018), http://github.com/google/jax.

[56] I. Babuschkin, K. Baumli, A. Bell, S. Bhupatiraju, J. Bruce, P. Buchlovsky, D. Budden, T. Cai, A. Clark, I. Danihelka, C. Fantacci, J. Godwin, C. Jones, R. Hemsley, T. Hennigan, M. Hessel, S. Hou, S. Kapturowski, T. Keck, I. Kemaev, M. King, M. Kunesch, L. Martens, H. Merzic, V. Mikulik, T. Norman, J. Quan, G. Papamakarios, R. Ring, F. Ruiz, A. Sanchez, R. Schneider, E. Sezener, S. Spencer, S. Srinivasan, L. Wang, W. Stokowiec, and F. Viola, The DeepMind JAX Ecosystem (2020), http://github.com/deepmind.

[57] L. Messio, C. Lhuillier, and G. Misguich, Phys. Rev. B **83**, 184401 (2011).

[58] We notice several complicated phases around the two SU(3) points at $(\theta/\pi, \phi/\pi) = (0.5, 0.25)$ and $(0.5, 0.5)$. These will be discussed elsewhere.

[59] I. Niesen and P. Corboz, SciPost Phys. **3**, 030 (2017).

[60] P. Corboz, M. Lajkó, K. Penc, F. Mila, and A. M. Läuchli, Phys. Rev. B **87**, 195113 (2013).

[61] A. M. Samarakoon, A. Banerjee, S.-S. Zhang, Y. Kamiya, S. E. Nagler, D. A. Tennant, S.-H. Lee, and C. D. Batista, Phys. Rev. B **96**, 134408 (2017).

[62] O. Tchernyshyov and G.-W. Chern, Spin-lattice coupling in frustrated antiferromagnets, in *Introduction to Frustrated Magnetism: Materials, Experiments, Theory*, edited by C. Lacroix, P. Mendels, and F. Mila (Springer, Berlin, Heidelberg, 2011), pp. 269–291.

[63] E. M. Stoudenmire, S. Trebst, and L. Balents, Phys. Rev. B **79**, 214436 (2009).

[64] M. E. Valentine, T. Higo, Y. Nambu, D. Chaudhuri, J. Wen, C. Broholm, S. Nakatsuji, and N. Drichko, Phys. Rev. Lett. **125**, 197201 (2020).

[65] A. Yoshimori and S. Inagaki, J. Phys. Soc. Jpn. **50**, 769 (1981).

[66] M. Hoffmann and S. Blügel, Phys. Rev. B **101**, 024418 (2020).

[67] R. Soni, N. Kaushal, C. Şen, F. A. Reboredo, A. Moreo, and E. Dagotto, New J. Phys. **24**, 073014 (2022).

[68] L. Janssen, E. C. Andrade, and M. Vojta, Phys. Rev. Lett. **117**, 277202 (2016).

[69] W. Yao, K. Iida, K. Kamazawa, and Y. Li, Phys. Rev. Lett. **129**, 147202 (2022).

[70] W. Chen, X. Li, Z. Hu, Z. Hu, L. Yue, R. Sutarto, F. He, K. Iida, K. Kamazawa, W. Yu, X. Lin, and Y. Li, Phys. Rev. B **103**, L180404 (2021).

[71] W. G. F. Krüger, W. Chen, X. Jin, Y. Li, and L. Janssen, arXiv:2211.16957.

[72] We have confirmed that our method reproduces the short-range spin correlations expected for the $S = 1$ Kitaev spin liquid [40] (see also Supplemental Material [49]).

[73] J. Nasu, Y. Kato, J. Yoshitake, Y. Kamiya, and Y. Motome, Phys. Rev. Lett. **118**, 137203 (2017).

[74] Y. Amari, Y. Akagi, S. B. Gudnason, M. Nitta, and Y. Shnir, Phys. Rev. B **106**, L100406 (2022).

[75] H. Zhang, Z. Wang, D. Dahlbom, K. Barros, and C. D. Batista, arXiv:2203.15248.

[76] X. Bai, S.-S. Zhang, Z. Dun, H. Zhang, Q. Huang, H. Zhou, M. B. Stone, A. I. Kolesnikov, F. Ye, C. D. Batista, and M. Mourigal, Nat. Phys. **17**, 467 (2021).

[77] U. F. P. Seifert and L. Savary, Phys. Rev. B **106**, 195147 (2022).

[78] R. Iwazaki, H. Shinaoka, and S. Hoshino, arXiv:2301.09824.

[79] G. Marsaglia, Ann. Math. Stat. **43**, 645 (1972).

[80] N. Metropolis, A. W. Rosenbluth, M. N. Rosenbluth, A. H. Teller, and E. Teller, J. Chem. Phys. **21**, 1087 (1953).

[81] R. H. Swendsen and J.-S. Wang, Phys. Rev. Lett. **57**, 2607 (1986).

[82] K. Hukushima and K. Nemoto, J. Phys. Soc. Jpn. **65**, 1604 (1996).

[83] D. J. Earl and M. W. Deem, Phys. Chem. Chem. Phys. **7**, 3910 (2005).